文章编号：1001－9014(2019)04－0408－04

DOI:10.11972/j.issn.1001－9014.2019.04.003

The effects of self-heating on mid-infrared interband cascade lasers grown on InAs substrates

YU Cheng-Zhang[1,2,3], XU Zhi-Cheng[1], CHEN Jian-Xin[1*], HE Li[1]

(1. Key Laboratory of Infrared Imaging Materials and Detector, Shanghai Institute of Technical Physics; Chinese Academy of Sciences, Shanghai 200083, China;
2. University of Chinese Academy of Sciences, Beijing 100049, China;
3. School of Physical Science and Technology, University of ShanghaiTech, Shanghai 201210, China)

Abstract: In this paper, InAs-based type-II interband cascade lasers operating at the mid-infrared range were fabricated and characterized. The maximum operating temperatures under pulsed and continuous wave (CW) operating mode are determined to be 275 K and 226 K, respectively. The threshold current density is around 17 A/cm^2 at 80 K with an emission wavelength of approximate 3.8 μm. We analyzed the self-heating effects under CW mode and further simulated the temperature contour by the finite element method. The results indicate that the self-heating effect is a critical factor that limits the operating temperature under CW mode for our devices. Further optimization of the heat dissipation performance would be an effective way to raise the operating temperature of these devices.

Key words: interband cascade lasers, mid-infrared rang, molecular beam epitaxy(MBE)
PACS: 42.55.Px, 78.67.Pt, 42.72.Ai

InAs基中红外带间级联激光器中的自加热效应

余成章[1,2,3], 徐志成[1], 陈建新[1*], 何 力[1]

(1. 中国科学院上海技术物理研究所 红外成像材料与器件重点实验室,上海 200083;
2. 中国科学院大学,北京 100049;
3. 上海科技大学 物质科学与技术学院,上海 201210)

摘要:制备并测试了II型中红外带间级联激光器,制备的器件在脉冲和连续工作模式下最高工作温度分别为275 K和226 K.80 K下器件激射波长为3.8 μm左右,阈值电流密度约17 A/cm^2.对器件在连续工作模式下的自加热效应进行了分析,并利用有限元方法模拟了器件连续工作时的温度分布图.分析和模拟结果均表明自加热效应是限制器件连续工作温度的重要因素.提高散热性能将是进一步提升器件工作温度的有效手段.

关 键 词:带间级联激光器;中红外;分子束外延

中图分类号:O43 **文献标识码**:A

Introduction

The concept of interband cascade lasers(ICLs) was proposed by R. Yang in 1994[1]. The ICLs have the advantages of cascade structure and interband carrier transition, promising for low threshold current and low power consumption[2]. The first ICL was demonstrated in 1997 with an emission wavelength of 3.8 μm[3]. It reached room temperature operation under pulsed mode in 2001[4], and under continuous wave (CW) mode in 2008[5]. Since then the structures of ICLs have been significantly improved. InAs/GaInSb/InAs "W" shaped quantum wells were used in the active core region to improve optical gain[6]. The strategy called carrier rebalancing significantly reduced threshold current density by increasing the doping concentration in the electron injector[7]. Up to now, the ICLs have shown excellent per-

Received date: 2018-08-30, **revised date**: 2019-05-24 **收稿日期**:2018-08-30, **修回日期**:2019-05-24
Foundation items:Supported by National Natural Science Foundation of China (61534006, 61290302, 61505237, 61404148), and the National Key Research and Development Program of China (2016YFB0402403)
Biography:YU Cheng-Zhang(1991-), male, Quzhou China, Ph. D, Research area is mid-IR interband cascade lasers. E-mail: yuchzh@shanghaitech.edu.cn
* **Corresponding author**:E-mail:jianxinchen@mail.sitp.ac.cn

formances in the mid-infrared (IR) region and have been successfully used in gas detection, environmental monitoring, and many other fields. In particular, in the Mars rover "curiosity" launched by National Aeronautics and Space Administration (NASA) of the United States of America, the spectrometer was equipped with an ICL[8].

Although the current ICLs have made significant progress, self-heating effect is still one decisive factor affecting their performances. Lots of exploration and efforts have been carried out by researchers on this issue. By measuring the thermal conductivity tensors of the cladding and active layers using 3ω method[9-10], it has been found that the poor heat dissipation in ICLs is mainly due to the low thermal conductivity of the InAs/AlSb cladding layers. Epitaxial side down (Epi-down) mounting is an effective method to alleviate this problem. Theoretical and experimental results showed that Epi-down mounting could realize a 4/3 improvement in thermal resistance[11]. Another way is to use the heavily doped InAs as cladding layers (called InAs-plasmon waveguide) instead of the InAs/AlSb superlattices cladding layers due to InAs's superior performance of thermal dissipation[12-13]. The thermal resistance measured for board area devices is about 16 K cm^2/kW for InAs-plasmon waveguide ICLs, comparable lower than 30 K cm^2/kW for InAs/AlSb waveguide devices[14-15]. In this paper, we studied the self-heating effect on InAs-based ICLs, and further obtained the actual temperature of the active region under CW operating mode by simulation. Firstly, we report the fabrication and characterization of InAs-based ICL, then we analyze the self-heating effect under CW operating mode by comparing the threshold current densities under pulsed and CW operating mode. Finally, the finite element method was used to simulate the self-heating effects.

1 Experiments

The ICL structure consists of ten cascade stages as the active core. Figure 1(a) shows the band edge diagram of one cascade stage, which consists of an electron injector, an active region and a hole injector from left to right. The electron injector is composed of InAs/AlSb multilayers. The mid four InAs wells in the electron injector are N-doped ($\sim 1.5\times10^{17}$ cm^{-3}) to act as an electron reservoir. The radiative transition takes place from the electron subband of the InAs layer to the hole subband of GaInSb layer in the active region. The holes are injected from the GaSb/AlSb multiple quantum wells. Highly Si-doped up to 1×10^{19} cm^{-3} InAs layers with a thickness of 1.6 μm which have lower refractive index than the core region, were used as both the bottom and top cladding layers. Two 1.15 μm thick undoped InAs spacers are grown between the cladding layers and the active core in order to reduce the free carrier absorption loss. Figures 1(b-c) depicts the layer structure and the refractive index diagram, as well as the optical mode profile[2]. The entire structure is grown by molecular beam epitaxy (MBE) with a growth temperature around 500℃. The growth rate is calibrated by in-situ reflection high energy electron diffraction (RHEED). The high-resolution X-ray diffraction measurement of the epitaxial structure is shown in Fig. 1(d). More than 30 sharp satellite peaks can be clearly observed. The inset of Fig. 1(d) shows the first three satellite peaks and the full width at half maximum (FWHM) of the minus 1st diffraction satellite peak was only 28.8, showing a high structural quality. The periodic thickness of the cascade structure is evaluated to be 571 Å, only 0.35% deviating from the design value, indicating a precise control of the material growth.

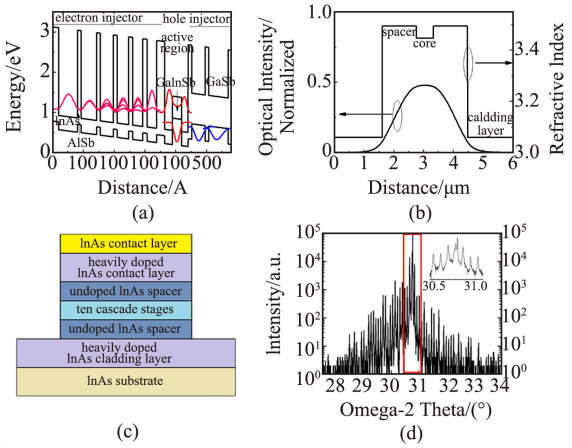

Fig. 1　(a) Diagram of band edge structure (b) optical mode profile and index profiles of the InAs plasmon enhanced waveguide, (c) InAs plasmon enhanced waveguide, (d) high-resolution X-ray diffraction rocking curve of the growth structure

图 1　(a) 单个级联周期的能带结构示意图,(b) InAs 等离子体波导结构的光学模式和折射率剖面图,(c) InAs 等离子体波导结构,(d)生长出材料的高分辨 X 射线衍射摇摆曲线

The epitaxy is then processed into ridge waveguide devices. Stripes with widths ranging from 18 to 25 μm are obtained by contact lithography and wet chemical etching. Figure 2(a) is a scanning electron microscopy (SEM) image of a device's facet with a ridge height of 20.6 μm, in which the top metal contact, cladding layers and spacers can be clearly observed. Moreover, a cross-sectional transmission electron microscope (TEM) image of a single cascade region is shown in Fig. 2(b), in which the electron injection, active region, and hole injection region are marked out. Both pulsed and continuous wave (CW) mode measurements were carried out on the fabricated devices. Light-current-voltage (*L-I-V*) measurements under pulsed mode were conducted on a home-made set-up using a mercury cadmium telluride (MCT) detector. The duty cycle is 0.5% with a pulse width of 1μs. The optical power under CW mode is measured by a power meter. The emission spectra at different temperatures are also measured by a Fourier Transform Infrared Spectrometer (FTIR).

2 Results and discussions

Figure 3 shows the emission spectra at different temperatures under both pulsed and CW modes. Under pulsed mode, the maximum operating temperature was

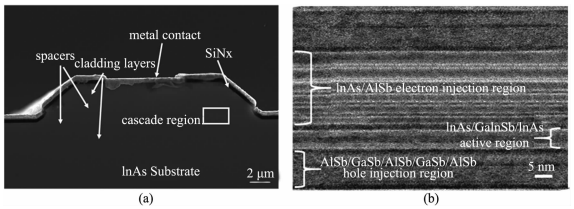

Fig. 2 (a) SEM image of a processed IC laser's facet, (b) cross-sectional TEM image of a single cascade region
图2 (a)制备好的带间级联激光器的腔面 SEM 图,(b)一个级联周期结构的 TEM 图

275 K. The emission wavelength shifted from 3.80 μm at 80 K to 4.14 μm at 275 K with a rate of 1.86 nm/K. While the maximum operating temperature under CW mode was 226 K with an emission wavelength of 4.11 μm. The emission wavelength under CW mode is longer than that under pulsed mode at the same heat sink temperature, which is caused by heat production from the continuous current injection, leading to a higher temperature at the active core region than the heat sink.

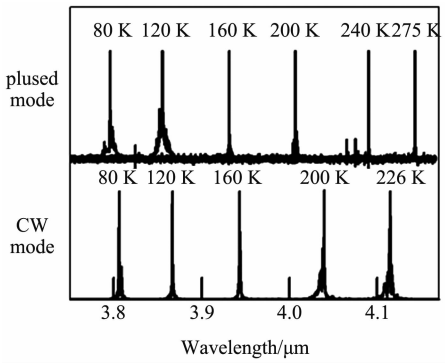

Fig. 3 Emission spectra under pulsed and CW operating mode at different temperatures
图3 脉冲和连续工作模式下不同温度的激射光谱

Figure 4 shows the dependence of the threshold current density of a device with a stripe width of 20.6 μm and a length of 3 mm at different heat sink temperatures under both pulsed and CW mode. Under pulsed mode it was 17.0 A/cm^2 at 80 K (17.2 A/cm^2 under pulsed mode), and increased to 1 091.1 A/cm^2 at 275 K. The threshold current densities under CW and pulsed mode were close to each other at temperatures below 200 K, while the values under two modes shows quite a difference when temperature is higher than 200 K, indicating that self-heating starts to become significant at such temperatures. This is consistent with the spectra measurements that the emission wavelength under CW mode is longer than that under pulsed mode at the same heat sink temperature. The relationship between threshold current density and temperature could be modeled as,

$$J_{th}(T) = J_{th}(T_0)e^{\frac{T}{T_0}} \quad (1)$$

where T_0 is the characteristic temperature, $T = T_{sink} + \Delta T$ means the actual temperature at the core region. ΔT is the temperature difference between the active core region and the heat sink. Under pulsed mode, ΔT is set to be 0, thus $T = T_{sink}$. The calculated result under pulsed mode was shown as the black solid line in Fig. 4. T_0 of 50.3 K between 80 K and 230 K was then obtained, which is a typical value of ICLs[16].

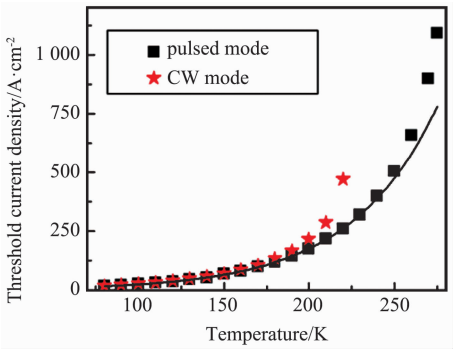

Fig. 4 Dependence of the threshold current density on the heatsink temperature under pulsed and CW operating mode
图4 脉冲和连续工作模式下阈值电流与热沉温度的依赖关系

Under CW operation, the continuously injected currents will produce a certain amount of Joule heat causing a temperature gradient from the active core to the heat sink. Figure 5(a) shows the temperature contour of an ICL's half facet simulated by the finite element method (FEM). The solid heat transfer model was used in this simulation. The heat source was set at the core region, the temperature of the copper heat sink was set as constant, and adiabatic boundary conditions were set at other boundaries. The thermal conductivity coefficients of 27 W/(m·K) for InAs and 1.5 W/(m·K) for the active core region was adopted[17]. The temperature difference ΔT between the active core and the heat sink at different heat sink temperatures obtained through FEM simulation is shown in Fig. 5(b) as the dotted dash red line. The temperature difference ΔT can also be estimated by comparing the temperatures at which the pulsed mode and CW mode have the same threshold currents assuming the Joule heat is negligible under pulsed mode. For doing so, we may go back to Fig. 4. At a certain heat sink temperature T_1, one may have a threshold current density under pulsed mode. For this threshold current density, one may then locate another temperature T_2 under CW mode. The $\Delta T(=T_2 - T_1)$ as a function of heat sink temperature is shown in Fig. 5(b) as black stars. The simulation results are well consistent with and the experimental data. For example, at a heat sink temperature of 220 K, the estimated ΔT by comparing threshold currents at the two operating modes is 29.3 K, and a similar value of 31.9 K was obtained by FEM simulation. It should be noticed that ΔT increases exponentially when the heat sink temperature is higher than 180 K. This is the major reason that the maximum CW operating temperature is 49 K lower than the maximum pulsed operation temperature. Advanced device processing methods, such as electroplating or Epi-side down mounting will help to increase the CW operating temperature.

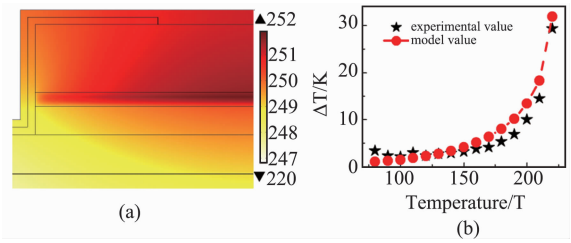

Fig. 5　(a) Temperature contour of an ICL's half face under the threshold at 220 K simulated by FEM method, (b) experimental value and model value of temperature difference between the active region and heat sink under CW mode

图 5　(a)利用有限元方法模拟得到 220 K 下刚达到阈值时器件一半腔面的温度分布图,(b)连续工作模式下刚达到阈值条件时,不同温度下有源区与热沉之间实验和模拟得到的温度差

3 Conclusions

In summary, we have grown high-quality InAs based type-II interband cascade lasers by MBE. The laser emission wavelength is around 4 μm, with a maximum operating temperature of 275 K under pulsed mode and 226 K under CW mode. The threshold current density at 80 K is 17.0 A/cm^2 under pulsed mode and 17.2 A/cm^2 under CW mode. At last, the self-heating at the active region under CW mode has been discussed. The results show that the self-heating effect would limit the device performance when operated above 180 K under CW mode. Further studies are underway on structure optimization and device packaging to elevate device performances.

Acknowledgments

This work in part was supported by National Natural Science Foundation of China (61534006, 61290302, 61505237 and 61404148), the National Key Research and Development Program of China (2016YFB0402403). The design of the interband cascade laser structure was provided by Prof. Rui Q. Yang of University of Oklahoma (OU). The authors are grateful to him and his research group at OU for discussion and help in ICL.

References

[1] Yang R Q. Infrared laser based on intersubband transitions in quantum wells[J]. *Superlattices and Microstructures*, 1995, **17**(1): 77 - 83.

[2] YANG Rui-Qing, LI Lu, JIANG Yu-Chao. Interband cascade lasers: From oringinal concept to practical devices[J]. *Progress in Physics* (楊瑞青, 李路, 江宇超. 带间级联激光器: 从原始概念到实际器件. 物理学进展), 2014, **34**(4): 169 - 190.

[3] Yang R Q, Zhang D, Murry S J, *et al*. Type-II interband quantum cascade laser at 3.8 ? m[J]. *Electronics Letters*, 1997, **33**(7): 598 - 599.

[4] Yang R Q, Bradshaw J L, Bruno J D, *et al*. Room temperature type-II interband cascade laser[J]. *Applied physics letters*, 2002, **81**(3): 397 - 399.

[5] Kim M, Canedy C L, Bewley W W, *et al*. Interband cascade laser emitting at λ = 3.75 μ m in continuous wave above room temperature [J]. *Applied Physics Letters*, 2008, **92**(19): 191110.

[6] Meyer J R, Hoffman C A, Bartoli F J, *et al*. Type - II quantum-well lasers for the mid - wavelength infrared[J]. *Applied physics letters*, 1995, **67**(6): 757 - 759.

[7] Vurgaftman I, Bewley W W, Canedy C L, *et al*. Rebalancing of internally generated carriers for mid-infrared interband cascade lasers with very low power consumption[J]. *Nature communications*, 2011, **2**: 585.

[8] Webster C R, Mahaffy P R, Atreya S K, *et al*. Mars methane detection and variability at Gale crater[J]. *Science*, 2015, **347**(6220): 415 - 417.

[9] Borca-Tasciuc T, Achimov D, Liu W L, *et al*. Thermal conductivity of InAs/AlSb superlattices[J]. *Microscale Thermophysical Engineering*, 2001, **5**(3): 225 - 231.

[10] Zhou C, Vurgaftman I, Canedy C L, *et al*. Thermal conductivity tensors of the cladding and active layers of antimonide infrared lasers and detectors[J]. *Optical Materials Express*, 2013, **3**(10): 1632 - 1640.

[11] Chryssis A, Ryu G, Dagenais M. Thermal impedance of epi-up and epi-down interband cascade lasers[C]//*in 23rd Annual Meeting of the IEEE Photonics Society. IEEE*, 2010: 421 - 422.

[12] Tian Z, Yang R Q, Mishima T D, *et al*. InAs-based interband cascade lasers near 6 μm[J]. *Electronics Letters*, 2008, **45**(1): 48 - 49.

[13] Tian Z, Chen C, Yang R Q, *et al*. InAs-based plasmon-waveguide interband cascade lasers[C]//*Novel In-Plane Semiconductor Lasers IX. International Society for Optics and Photonics*, 2010, **7616**: 76161B.

[14] Yang R Q, Hill C J, Yang B H. High-temperature and low-threshold midinfrared interband cascade lasers [J]. *Applied Physics Letters*, 2005, **87**(15): 151109.

[15] Tian Z, Yang R Q, Mishima T D, *et al*. Plasmon-waveguide interband cascade lasers near 7.5 μm[J]. *IEEE Photonics Technology Letters*, 2009, **21**(21): 1588 - 1590.

[16] Olafsen L J, Aifer E H, Vurgaftman I, *et al*. Near-room-temperature mid-infrared interband cascade laser [J]. *Applied physics letters*, 1998, **72**(19): 2370 - 2372.

[17] Chryssis A N. Design and fabrication of high-performance interband cascade tunable external cavity lasers[D]. 2010.